Optic disc and macula detection in fundus images by means of template matching

Tzolkin Garduno-Alvarado[1] M. Elena Martinez-Perez[1] Maria A. Martinez-Castellanos [2]
Luvia Rodriguez-Quinones[2] Samantha M. Salinas-Longoria[2]

***Abstract*— Various methods for detecting optic disc and macula in fundus images have been developed. Our aim is to propose a fairly easy method for detecting both features jointly. This is achieved by first correcting inhomogenous luminosity using a polynomial approximation of the background of the images. Secondly, the use of the cross-correlation in the frequency domain between the images and a steerable template which contains both structures. The 38 photographs used in this work belong to a local database of patients suffering diabetic retinopathy along its four severity stages. Our results showed 100% optic disc centers located within the OD area and 90% macula centers located within the MC area.**

I. INTRODUCTION

Diabetic Retinopathy (DR) is a chronic disease that affects the eye. More specifically, it is the manifestation of *diabetes mellitus* in the eye retina. It is catalogued by the World Health Organization as one of the principal pathologies causing blindness, [23]. Fundus images, Fig. 1, are used as a tool for analyzing the progression of DR. With the aid of fundus images, opththalmologists can trace and locate lessions caused by DR. The amount and localization of these lessions determines the severity of the disease, [5], thus a reference point is needed to grade fundus images. Typically, the reference system is a cartesian plane with the center of the *optic disc* as origin, the abscissa being the line through the center of the *macula*.

Fig. 1: Color fundus image

The OD is a retinal area mildly oval with the major axis in the vertical position. Its mean area is 2.7 mm^2 and its horizontal radius of aproximately 1.8 *mm*. The variability of OD size is wide, its area can vary by a factor of 7, its horizontal diameter by a factor of 2.5, [13]. OD color can be yellowish orange with the temporal half a bit paler. The nasal half of the OD has a less delineated edge, [13]. The main dificulty for OD location achievement in a fundus image is the presence of objects that share characteristics with the OD such as intensity, color or variations in the reflection coefficient [22]. There is a wide variety of methods implemented for the location and segmentation of the OD, [9], [22], [4], namely: (1) searching of an area with the highest intensity variation for the location of the OD, [18], [6], [17], (2) searching of an area that resembles an OD template, [6], [15], (3) identifying the OD by means of the selection of the largest region that contains high intensity values, (4) estimating the OD edge using the Hough transform, [14], [6], [17], (5) estimation of the convergence of the retinal vasculature, [7], [6], [19], [24], [15], [21], (6) Hausdorff based matching, [12], (7) principal component analysis, [2], [1].

The MC is an oval area in the center of the retina. It is located 3 to 4 mm (15 degrees) from the OD, slightly downward, and between the major temporal vascular arcades. Its shape is circular and its diameter is approximately the same as the OD [13]. Under white light coloring, it appears darker than the retina. Its coloration presents low contrast when compared to the surrounding tissue, so the delimitation of a border becomes complicated. Blood vessels are used as reference for estimating the MC position, [19]. Location of the MC is commonly done by detecting its center. It is not usually segmented given its border is not clearly defined. Some of the methods used for MC location are (1) intensity variation and template matching, [18], [15], [17], (2) principal component analysis and active shape models, [14], (3) region growing, [6], (4) parabola adjustment to principal arcade, [19], (5) kNN regresion classifier, [15], (6) morphologial operators, [17], (7) arcade segmentation, [17], [8], [20].

In this paper we propose the automatic detection of OD and MC using a fairly simple method based on template matching. Using the anatomical property that these two structures have, the search pattern characterizes both structures at the same time. The algorithm also allows to discern between right and left eye during the detection process. It works in images OD centered as well as in MC centered, as far as both structres are present in the image.

[1]Department of Computer Science. Institute of Research in Applied Mathematics and Systems. Universidad Nacional Autónoma de México. Cicuito Escolar 3000, Ciudad Universitaria, México D.F. Apartado Postal 20-126, C.P. 01000.

[2]Asociaciń para Evitar la Ceguera en México I.A.P Hospital "Dr. Luis Sánchez Bulnes". Vicente García Torres 46, Colonia Barrio San Lucas, Delegación Coyoacán, Mexico D.F. C.P 04030

978-1-4244-7929-0/14/$26.00 ©2014 IEEE

II. MATERIALS

The set of images used in this paper consists of 38 images corresponding to either left or right eyes from patients suffering from diabetic retinopathy, Fig. 1. All the images were captured with a Carl Zeiss FF450 plus IR fundus camera, the field of view angle used is 50 degrees and the size of the images is 489×647 pixels. All the photographs are saved in non compressed *bmp* format. The totality of the images have had the OD and MC structures segmented by two licensed ophthalmologists, such segmentations are used as the gold standard for latter evaluation.

III. ALGORITHM

The fundus image database along with the manual segmentation (MS) for each specialist is under construction. Since we have 38 images so far and we require training and testing sets, then the overall detection process performs a k-fold cross validation on the set of images. The starting point of a k-fold cross validation is dividing the set of images into k roughly equal and mutually exclusive subsets. A loop of k iterations is then executed, in each iteration $k-1$ of the subsets are used for training, while the remaining one is used for validation. Each subset is validated in only one iteration, whilst it is used $k-1$ times for training, [11], [3]. On our algorithm, each iteration is divided into three stages, say training, determination of a region of interest and validation. A brief description of these stages is given below.

A. Preprocessing

Before running the algorithm, a noise reduction median filter is applied to the green band of the images, kernel size being 4×4. Each image presents a non-uniform illumination given the environmental conditions of the eye fundus imaging as well as the intrinsic dynamics of the ligth path inside the eye. A polynomial approximation of the background illumination was made using a basis of discrete orthogonal polynomials, [16], [10], the polynomials used for the present approximation were of third degree. Next, the approximation was subtracted from the original image. Fig. 2(a) shows the result of this process.

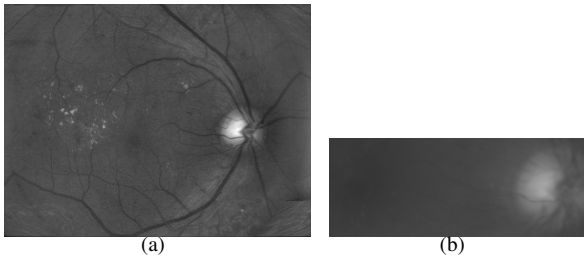

(a) (b)

Fig. 2: (a) Result of the subtraction of the polynomial approximation from the green band of the image. (b) Example of output template from the training stage.

B. Training

The aim of training is to build a template. The training step of each iteration of the k-fold cross validation loop of our algorithm receives t images as input. The output is a grayscale template of the region where the OD and MC are located and two angles α and σ. Notice the template is designed to contain both features and will be used without making an explicit separation of them. The MS of the two ophthalmologists are used as reference to devise the template. Each image I_j, $j = 1,2,...,t$, $t = 38$, has a subimage extracted, which contains the area where the MS of both features was made, let T_j be that subimage. T_j is rotated $-a_j$ degrees, where a_j corresponds to the angle drawn by the horizontal line and the one containing the OD and MC centroids in I_j, the interpolation used was bicubic. Angle α is assigned the mean value of a_j and σ its standard deviation. The images obtained are cropped to the size of the smallest T_j. From the latter set, an average image T is obtained, T is the output template, Fig. 2(b).

C. Validation

During this stage, the process of template matching is carried out, it returns a subimage of each image I_j on the validation set in question. For this purpose, six templates, namely T_r, $r = 1,2,...,6$, are created. These templates are such that $T_1 = rot(T,\alpha)$, where $rot(T,\alpha)$ is an α degree rotation of T, $T_2 = rot(T,\alpha+\sigma)$, $T_3 = rot(T,\alpha-\sigma)$, $T_4 = flip(T_1)$, where $flip(T_1)$ is a flipping of T_1 along the vertical axis, $T_5 = flip(T_2)$ and $T_6 = flip(T_3)$.

Let $j = j_0$ be fixed and such that I_{j_0} belongs to the validation set. The first step towards finding an area of interest in I_{j_0} is to perform a cross-correlation. The cross-correlation between two functions $f : \mathbb{R}^2 \to \mathbb{R}$ and $g : \mathbb{R}^2 \to \mathbb{R}$ is defined as,

$$(f \star g)(x,y) = \sum_{m=-\infty}^{\infty} \sum_{n=-\infty}^{\infty} f(m,n) g^*(x+m, y+n), \qquad (1)$$

where $*$ denotes complex conjugation. Cross correlation measures the similarity between f and g on each point. Analogous to the convolution theorem, the cross-correlation in Fourier domain satifies

$$F(f \star g) = [F^*(f)]F(g), \qquad (2)$$

where F denotes a discrete Fourier transform. Next, six cross correlation matrices M_r, are computed:

$$M_r = F(I_{j_0}) \circ F^*(T_r), \qquad (3)$$

where $\circ$ denotes an element-wise product of matrices. Fig. 3(a)(c) display the matrix for the cross correlation of a right and left eye in Fig. 3(b)(d) with templates T_2 and T_4 respectively. The maximum value m_r of M_r is computed along with its corresponding coordinates (x_r, y_r). Each coordinate point (x_r, y_r) represents the center of a rectangular region the size of T_r where the similarity of T_r and I_{j_0} is the maximum. Thus the coordinates corresponding to $m = max(m_r)$ are chosen as the center of a rectangle R where the OD and MC lie. Suppose $r = r_0$ is such that $m = m_{r_0}$.

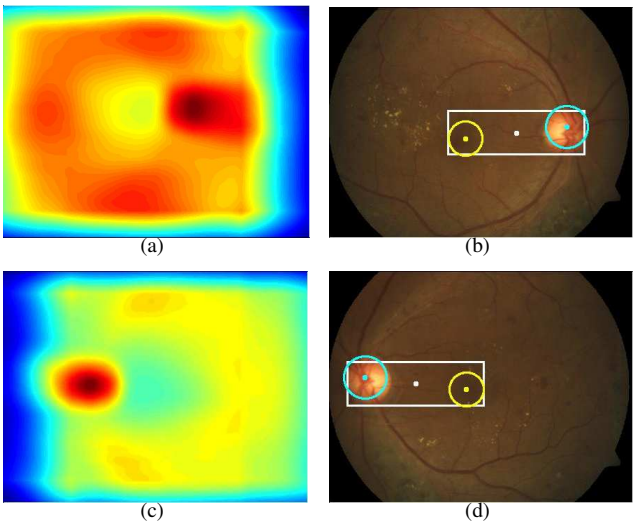

Fig. 3: (a) Cross correlation matrix for a right eye. (b) The yellow dot is the MC center, M_1, the cyan dot is the OD center, O_1, and the white dot is where m is found in the cross correlation. (c) Cross correlation matrix for a left eye eye. (d) Same as (b) for left eye.

Once R has been found in I_{j_0}, the OD and MC centroids are marked using the average centroids of the OD and MC relative to R. These points are then rotated $-\gamma$ degrees with the center point of R as the origin, where γ is such that $T = rot(T_{r_0}, -\gamma)$ for $r_0 = 1,2,3$ and $T = flip(rot(T_{r_0}, -\gamma))$ for $r_0 = 4,5,6$, let O_{j_0} and M_{j_0} be the resulting centroids of the OD and MC after the rotation. Afterwards, a circle is drawn with center O_{j_0} and radius the average of the OD radius of the training set. Similarly, a circle is drawn for the MC. Fig. 3(b)(d) show the results obtained for a right and left eye. Finally, the orientation of the eye is determined according to the template where the maximum cross-correlation was found. If it comes from T_r, $r = 1,2,3$, then the eye in question is right, otherwise it is left.

IV. Evaluation

The evaluation of the algorithm is a process with which the optimal k for the fold is chosen. Let O_j^1 and M_j^1 be the centroids of the OD and MC MS from the first specialist and O_j^2 and M_j^2 the respective centroids for the second one and let $P_i(k)$, $i = 1,...,4$, be the averages of $\{d(O_j, O_j^1)\}$, $\{d(O_j, O_j^2)\}$, $\{d(M_j, M_j^1)\}$ and $\{d(M_j, M_j^2)\}$ respectively, where d is the euclidean distance measured in pixels, $j = 1,...,t$ and O_j and M_j are the results of a k-fold cross-validation. In Figure 4(a) $P_1(k)$ and $P_2(k)$ are depicted for each $k = 2,...,19$ as blue and red lines with diamonds, $P_3(k)$ and $P_4(k)$ as blue and red lines with circles. Notice that P_1 and P_2 are almost entirely overlapped, this is due to the low variation between specialists.

To calculate the total error $E(k)$, i.e. the appointed error for each k, the average of $\{P_i(k)\}$, $i = 1,...,4$, is estimated, Fig. 4(a) illustrates E as a magenta line with squares. Thus the value k for which E holds the minimum value is optimal for the fold. In this case, $k = 3$ is such value.

Once the optimal value $k = 3$ has been found, the algorithm was run over all the images and an estimation of the error for each image was made. In Fig. 4(b) a plot of $d(O_j, O_j^1)$ and $d(O_j, O_j^2)$ for $k = 3$ is shown. The magenta line determines the OD radius, this means that the distance of our result for OD was actually determined inside the OD area. Analogously, Fig. 4(c) shows the results for the MC. In this case, note that there are four images for which M_j was found outside the MC MS area by one specialist.

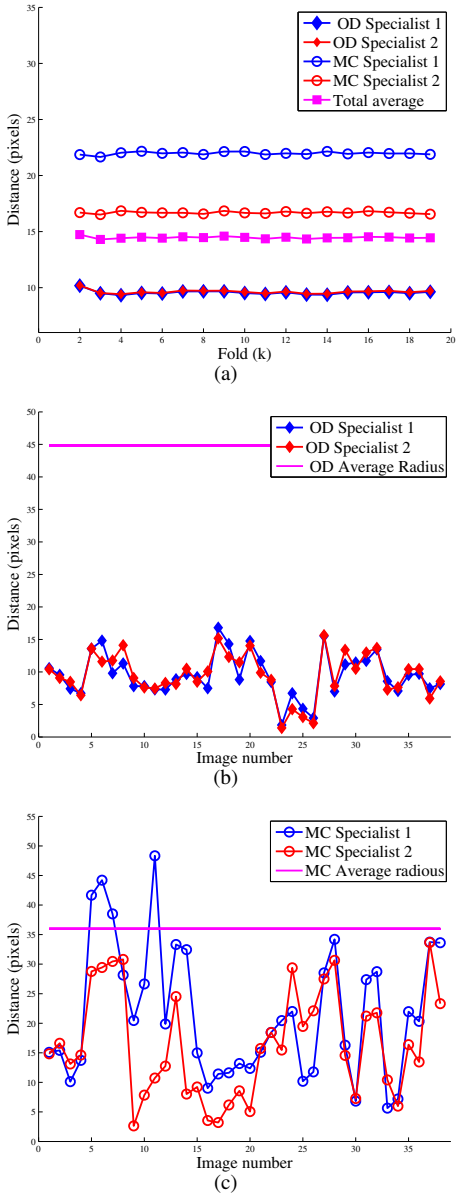

Fig. 4: (a) P_1 is the blue line with diamonds, P_2 is the red line with diamonds, P_3 is blue line with circles, P_4 red line with circles, E is the magenta line with squares. (b) $\{d(O_j, O_j^1)\}$ in blue and $\{d(O_j, O_j^2)\}$ in red for $k = 3$. (c) $\{d(M_j, M_j^1)\}$ in blue and $\{d(M_j, M_j^2)\}$ in red for $k = 3$.

V. Discussion

The method used for determining a region for the OD and MC applied in this paper is rather simple and easy to implement. Its goal has been achieved satisfactorily, nonetheless, an amelioration of the results could be made. One of the questions raised after the execution and result analysis is if the usage of discrete orthogonal polynomials of order three yielded the best approximation of the background of the image. Say fourth degree polynomials are used instead, is there a way to determine the optimal polynomial degree for the best backgound approximation? Another question in hand is how to determine k to avoid overfitting. The size of the image set used for this algorithm is small if compared with the amount of clinical images taken daily at a hospital. However small our set is, we think it is representative of the typical lesions found in eye fundus. For example several retinas showing photocoagulation marks have been included in our set, Fig. 5, this kind of lesions can be misleading when searching for the OD given the luminosity they present. Other lesions that can lead to errors are hard and soft exudates, their intrinsic coloration and brightness is very similar to that of the OD. Several images with this kind of lesions were included in our image set and neither was marked incorrectly. The difference between the MS of both specialists was not taken into consideration while evaluating. This difference is noticeable from Fig. 4(c) where the distance from the MC center result to the centroid of the MS of one specialist can be rather short while the distance to the second specialist may differ in up to 40 pixels, such difference represents 8% of our images height. For future work we have thought of performing an adjustment of the MC center by means of a local search. Additionaly, we will perform a segmentation of the OD and MC. Plus, we will increase our database size to improve our statistics. Finally, we will test our algorithm using some public datasets to make our method more reliable.

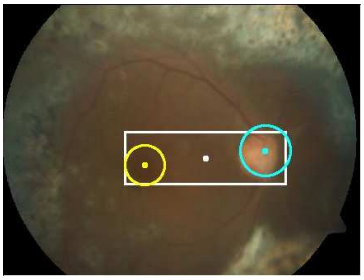

Fig. 5: Example of an eye with photocoagulation marks. The results of the algorithm on this image are shown.

Acknowledgement

This work was financially supported by PAPIIT project number IN103414 from UNAM, Mexico.

References

[1] M. Abramoff, W. Alward, E. Greenlee, L. Shuba, C. Kim, J. Fingert, and Y. Kwon. Automated segmentation of the optic disc from stereo color photographs using physiologically plausible features. *Investigative Ophthalmology and Visual Science*, 48(4):1665–1673, 2007.

[2] M. Abramoff, M. Garvin, and M. Sonka. Retinal imaging and image analysis. *IEEE Reviews in Biomedical Engineering*, 3:169–208, 2010.

[3] E. Alpaydin. *Introduction to Machine Learning*. The MIT Press, 2009.

[4] R. Bernardes, P. Serranho, and C. Lobo. Digital ocular fundus imaging: A review. *Ophthalmologica*, (226):161–181, 2011.

[5] Early Treatment Diabetic Retinopathy Study Research Group. Grading diabetic retinopathy from stereoscopic color fundus photographs: an extension of the modified Airlie House classification. *Ophtalmology*, (98):786–806, 1991.

[6] D. A. Fleming, A.K. Goatman, S. Philip, A.J. Olson, and F.P. Sharp. Automatic detection of retinal anatomy to assist diabetic retinopathy screening. *Phys. Med. Biol.*, 52(2):331–345, 2007.

[7] M. Foracchia, E. Grisan, and A. Ruggeri. Detection of optic disc in retinal images by means of a geometrical model of vessel structure. *IEEE Trans Med Imaging*, 10(23):1189–1195, 2004.

[8] M. Gegundez-Arias, D. Marin, J. Bravo, and A. Suero. Locating the fovea center position in digital fundus images usingthresholding and feature extraction techniques. *Comput. Med. Imaging Graph.*, (xx):xx, 2013.

[9] F. Haar. Automatic localization of the optic disc in digital colour images of the human retina. Tesis maestria, Utrech University, 2005.

[10] M. Harker and P. O'Leary. 2d polynomial data modelling: Version 1.0. http://www.mathworks.com/matlabcentral/fileexchange/42474-2d-polynomial-data-modelling-version-1-0/content/dop2DBoxV1-0/documentation/Sources/html/dop2DIlluminationDemo.html, February 2014. Institute for Automation, University of Leoben.

[11] R. Kohavi. A study of cross-validation and bootstrap for accuracy estimation and model selection. In *Proceedings of the 14th international joint conference on Artificial intelligence*, volume 72, pages 1137–1143, 1995.

[12] M. Lalonde, M. Beaulieu, and L. Gagnon. Fast and robust optic disc detection using pyramidal decomposition and Hausdorff based template matching. *IEEE Trans Med Imaging*, 11(20):1193–200, 2001.

[13] G.K. Lang. *Ophthalmology A Short Textbook*. Thieme, 2000.

[14] H. Li and O. Chutatape. Automated feature extraction in color retinal images by a model based approach. *IEEE Trans Biomed Eng*, 51:246–254, 2004.

[15] M. Niemeijer and B. Abramoff, M.D.and Van-Ginneken. Fast detection of the optic disc and fovea in color fundus photographs. *Medical Image Analysis*, (13):859–870, 2009.

[16] P. O'Leary and M. Harker. Discrete polynomial moments and savitzky-golay smoothing. In *Waset Special Journal*, volume 72, pages 439–443, 2010.

[17] R. Qureshi, L. Kovacs, B. Harangi, B. Nagy, T. Peto, and A. Hajdu. Combining algorithms for automatic detection of optic disc and macula in fundus images. *Computer Vision and Image Understanding*, 116:138–145, 2012.

[18] C. Sinthanayothin, J.F. Boyce, H.L. Cook, and T.H. Williamson. Automated localization of the optic disc, fovea, and retinal blood vessels from digital color fundus images. *Br J Ophthalmol*, 8(83):902–910, 1999.

[19] K.W. Tobin, E. Chaum, V.P. Govindasamy, and T.P. Karnowski. Detection of anatomic structures in human retinal imagery. *IEEE Trans Med Imaging*, 12(26):1729–1739, 2007.

[20] E. Trucco, K.S. Chin, Tanl L., and P.J. Wilson. Automatic fovea location in retinal images using anatomical priors and vessel density. *Pattern Recognition Letters*, 34:1152–1158, 2013.

[21] D. Welfer, J. Scharcanski, C. Kitamura, M. Pizzol, I. Ludwig, and D. Marinho. Segmentation of the optic disk in color eye fundus images using an adaptive morphological approach. *Comput Biol Med*, 40:124–137, 2010.

[22] R.J. Winder, P.J. Morrow, I.N. McRitchie, J.R. Bailie, and P.M. Hart. Algorithms for digital image processing in diabetic retinopathy. *Comp Med Imaging Graph*, 8(33):608–622, 2009.

[23] World Health Organization, International Agency fo the Prevention of Blindness. *Vision 2020 The Right to Sight. Global Initiative for the Elimination of Avoidable Blindness. Action Plan 2006-2011*. WHO, 2007.

[24] A. Youssif, A. Ghalwash, and A. Ghoneim. Optic disc detection from normalized digital fundus images by means of a vessels direction matched filter. *IEEE Transactions on Medical Imaging*, 27(1):11–18, 2008.